Multigrid for solving complex-valued Helmholtz problems

Isidoor Pinillo Esquivel

December 6, 2023

1 Indefinite Helmholtz equation

1.1 Discretization

(a)

$$10 \leq \lambda \ \#\text{gridpoints} \Leftrightarrow \tag{1}$$

$$10 \leq \frac{2\pi}{\sqrt{|\sigma|}} \frac{1}{h^d} \Leftrightarrow \tag{2}$$

$$\sqrt{|\sigma|} h^d \leq \frac{2\pi}{10} \approx 0.625. \tag{3}$$

(b)

$$\#\text{ gridpoints} = \frac{10\sqrt{600}}{2\pi}.$$

1.2 1D model problem

(a)
To proof : $H^{2h} \neq I_h^{2h} H^h I_{2h}^h$.

$$H^{2h} = H_n = A_n + \sigma I_n \tag{4}$$

$$H^h = H_{2n} = A_{2n} + \sigma I_{2n} \tag{5}$$

Assume that $A_n = I_h^{2h} A_{2n} I_{2h}^h = R_{2n} A_{2n} P_n$. By linearity it is sufficient to proof:

$$\sigma I_n \neq \sigma R_{2n} I_{2n} P_n \Leftrightarrow \tag{6}$$

$$I_n \neq R_{2n} I_n \Leftarrow \tag{7}$$

$$(I_n)_{00} = 1 \neq \frac{3}{4} = (R_{2n} P_n)_{00} \tag{8}$$

First equivalence follows from $\sigma \neq 0$. The assumption and the last inequality depends on the definition of restriction and interpolation.
(b)
We implemented $f(t) = \delta(t - 0.5)$ by concentrating all the mass into the middle

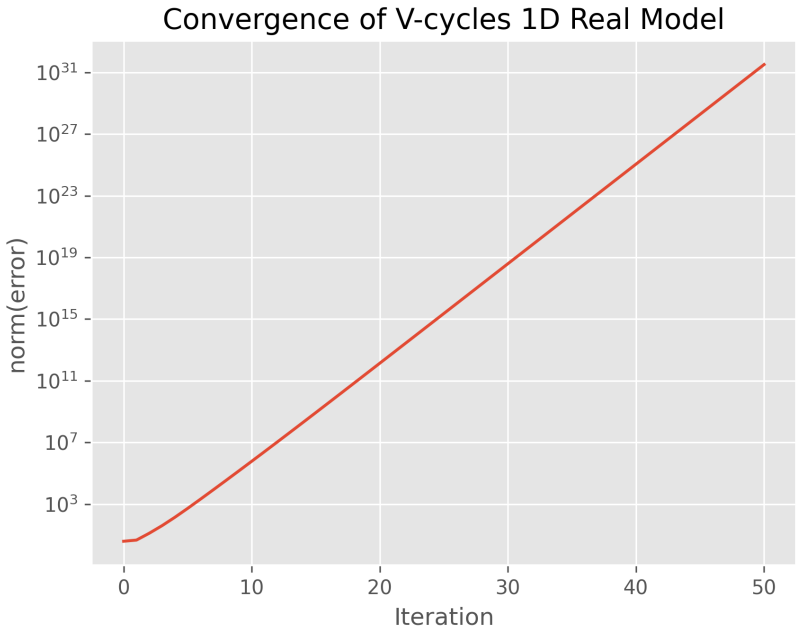

Figure 1: Convergence behavior of the V-cycles for solving the discretized Helmholtz equation with $\sigma = -600, n = 64$. The V-cycles seems to diverge, suggesting challenges in solving the Helmholtz problem using this approach.

element of f_n.

(c)
The eigenvalues and eigenvectors can be derived from the Poisson problem ($\sigma = 0$) because

$$Av = \lambda v \Rightarrow \tag{9}$$
$$(A + \sigma I)v = Av + \sigma v \tag{10}$$
$$= (\lambda + \sigma)v \tag{11}$$

i.e. eigenvectors stay the same and eigenvalues get shifted by σ.

(d)
$\sigma = 0$ is the boundary where H goes from indefinite to definite.

1.3 LFA analysis of the ω-Jacobi smoother

(a)
For grid points without a neighboring boundary point there H acts like following stencil:

$$H_n = n^2[-1 \quad 2 + \frac{\sigma}{n^2} \quad -1].$$

So R_ω works element wise the following way on the error:

$$e_j^{m+1} = (1 - \omega)e_j^m + \frac{\omega n^2}{2n^2 + \sigma}(e_{j-1}^m + e_{j+1}^m). \tag{12}$$

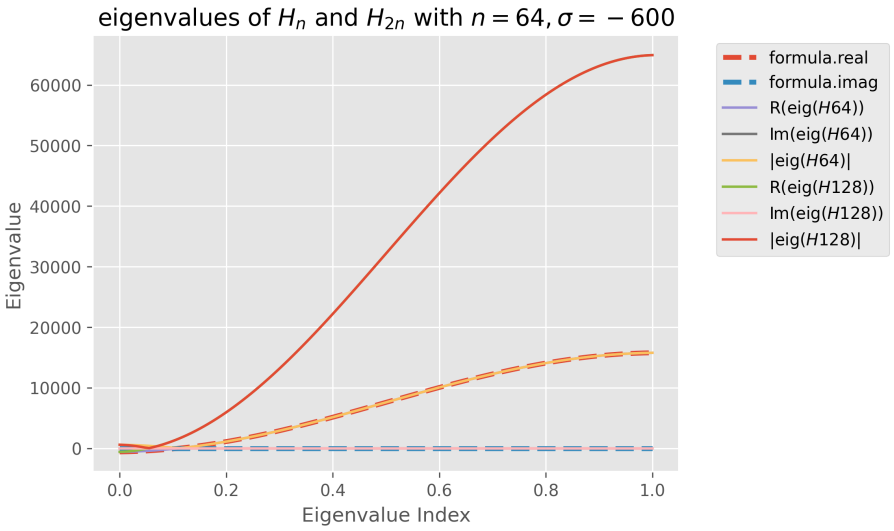

Figure 2: We sorted the eigenvalues and scaled the x-axis to make it easier to compare eigenvalues. Note that H_{2n} has twice the amount of eigenvalues then H_n.

The LFA analysis for the Helmholtz equation is very similar to the analysis for the Poisson equation. Doing the LFA subsitution $e_j^{(m)} = \mathcal{A}(m)e^{ij\theta}$:

$$A(m+1) = A(m)\left(1 - \omega + \frac{\omega n^2}{2n^2+\sigma}(e^{-i\theta} + e^{i\theta})\right) \tag{13}$$

$$= A(m)\left(1 - \omega + 2\cos(\theta)\frac{\omega n^2}{2n^2+\sigma}\right) \Rightarrow \tag{14}$$

$$G(\theta) = \left(1 - \omega + 2\cos(\theta)\frac{\omega n^2}{2n^2+\sigma}\right) \tag{15}$$

Note that we haven't used that σ is real.
(b)
$\sigma = 0$ reduces back to the LFA we did for the Poisson equation. $\theta \approx 0 \Rightarrow \cos(\theta) \approx 1 + O\left(\frac{1}{n^2}\right) \Rightarrow G(\theta) \approx 1 - O\left(\frac{1}{n^2}\right)$ so smooth modes are preserved for big n. For $\sigma < 0$ $G(\theta)$ becomes slightly bigger than 1 i.e. smooth modes get amplified.

(d)
Maximum of $G(\theta)$ is achieved at $\theta = 0$ because $G(\theta)$ is just an increasing function of $\cos(\theta)$ then try the minima and maxima of *cos*. This means that $\rho = |1 - \omega + 2\frac{\omega n^2}{2n^2+\sigma}| \approx 1.05$ which suggests that in the worst case the smoother my amplify error with a factor of 1.05.

1.4 Spectral analysis of the two-grid correction scheme

(a)
It is easily seen that

$$R_{2n} = cS_{2n}(3I_{2n} - A_{2n}). \tag{16}$$

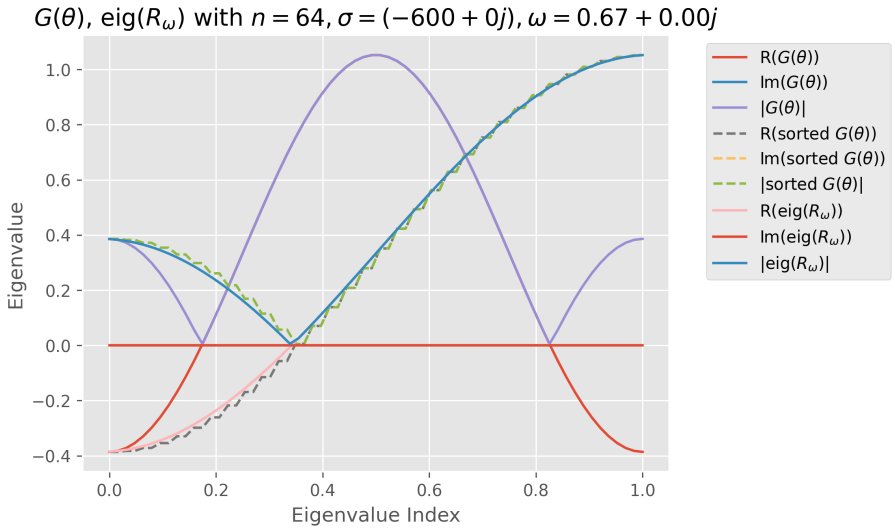

Figure 3: We sorted the eigenvalues and scaled the x-axis to make it easier to compare eigenvalues.

with $c \in \mathbb{R}_0$, $S_{2n} : \mathbb{R}^{2n-1} \to \mathbb{R}^{n-1} : (v_j)_{j \leq 2n-2} \to (v_{2j+1})_{j \leq n-2}$ subsampling uneven components. Using that $S_{2n} w_k^{2n} = w_k^n$ if $k < n$ it is easily seen that:

$$\begin{aligned} R_{2n} w_k^{2n} &= c S_{2n}(3I_{2n} - A_{2n}) w_k^{2n} && (17)\\ &= c(3 - \lambda_k(A_{2n})) S_{2n} w_k^{2n} && (18)\\ &= a(n,k) w_k^n. && (19) \end{aligned}$$

Good interpolation has by definition low reconstruction error. In our case P_n is linear interpolation, reconstuction error for lagrange interpolation can be bounded using Taylors theorem.

$$P_n S_{2n} v_{2n} \approx c v_{2n}. \tag{20}$$

For w_k^{2n} smooth and combining with previous argument we have:

$$P_n R_{2n} w_{2n} \approx c_1 w_{2n}. \tag{21}$$

To check the normalizing constant try $v_{2n} = 1 \Rightarrow c_1 = 1$.
Now doing spectral analysis of TG is straight forward:

$$\begin{aligned} TG w_k^{2n} &= (I_n - P_n H_n^{-1} R_{2n} H_{2n}) w_k^{2n} && (22)\\ &= w_k^{2n} - P_n H_n^{-1} R_{2n} \lambda_k(H_{2n}) w_k^{2n} && (23)\\ &= w_k^{2n} - P_n H_n^{-1} a(n,k) w_k^n \lambda_k(H_{2n}) && (24)\\ &= w_k^{2n} - P_n a(n,k) w_k^n \lambda_k(H_n^{-1}) \lambda_k(H_{2n}) && (25)\\ &= w_k^{2n} - P_n R_{2n} w_k^{2n} \lambda_k(H_n^{-1}) \lambda_k(H_{2n}) && (26)\\ &\approx w_k^{2n} - w_k^{2n} \lambda_k(H_n^{-1}) \lambda_k(H_{2n}) && (27)\\ &\approx w_k^{2n}(1 - \lambda_k(H_n^{-1}) \lambda_k(H_{2n})). && (28) \end{aligned}$$

(b)
We already analytically derived the eigenvalues for H_n.

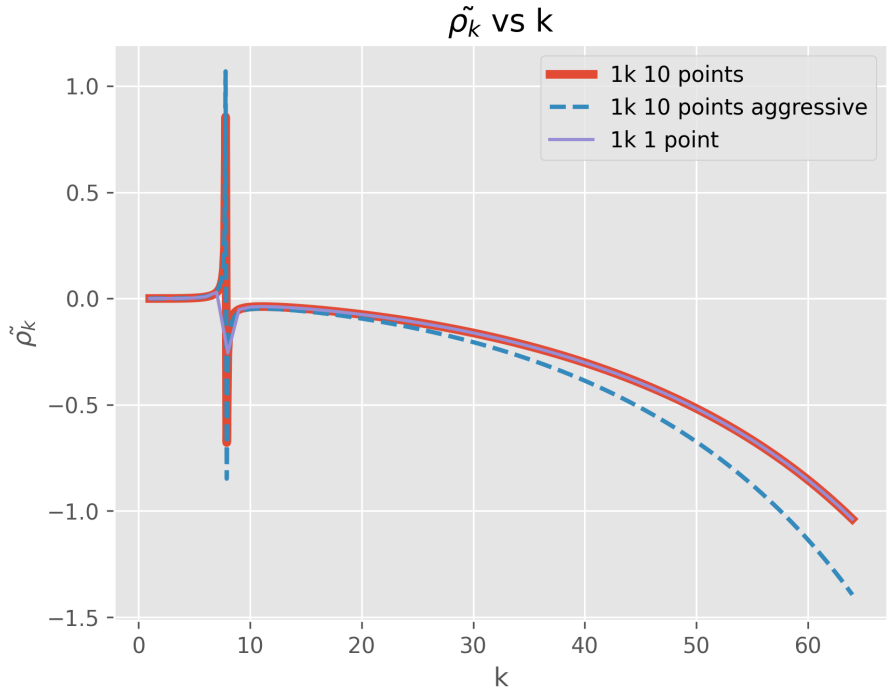

Figure 4: The spike represents the bad behavior of TG for the Helmholtz problem.

Sometimes a specific smooth eigenmode doesn't get dampend or even amplified by a TG iteration which is undesired.
(c)
See Figure 2. Obviously when the signs of $\lambda_k(H_n^{-1})$ and $\lambda_k(H_{2n})$ leads to $\tilde{\rho_k}$ which explains the spike. For $n = 64$ and $\sigma = -600$ the index closest to the sign change is $k = 6$. No, the smoother leaves smooth modes almost unchanged.

Combining the poor predicted performance of the smoother and TG-iteration it is not surprising that the V-cycles diverged.

2 Solving the complex-valued Helmholtz problem using Multigrid

2.1 1D model problem

(a)
For $\sigma = -600 - 300j, n = 64$ the problem does converges.
(b)
For a point source it was not be obvious so we used $f_n = w_{10}^n$ but the solution for the complex shifted problem is very similar.
(c)
We already analytically derived the eigenvalues for H_n. Again the spectrum get shifted by the complex shift.

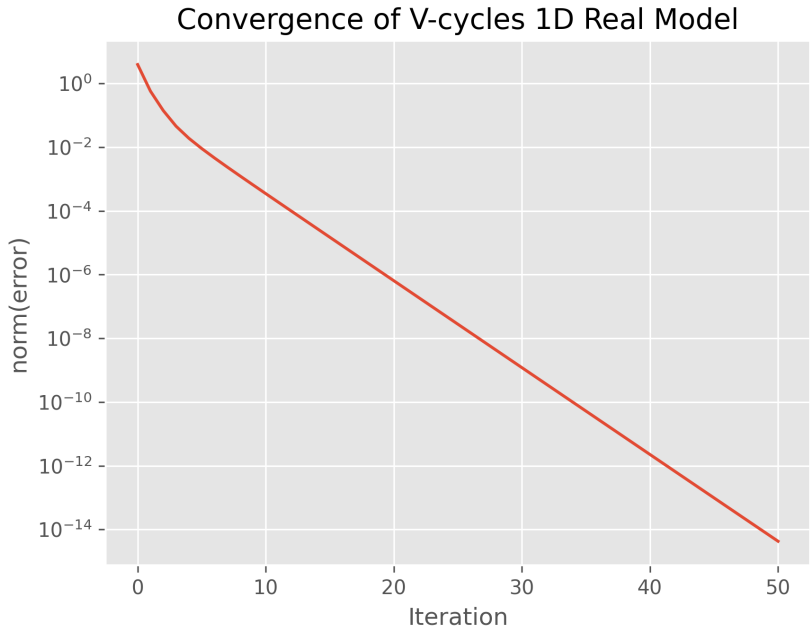

Figure 5: Convergence behavior of the V-cycles for solving the discretized Helmholtz equation with $\sigma = -600 - 300j, n = 64$.

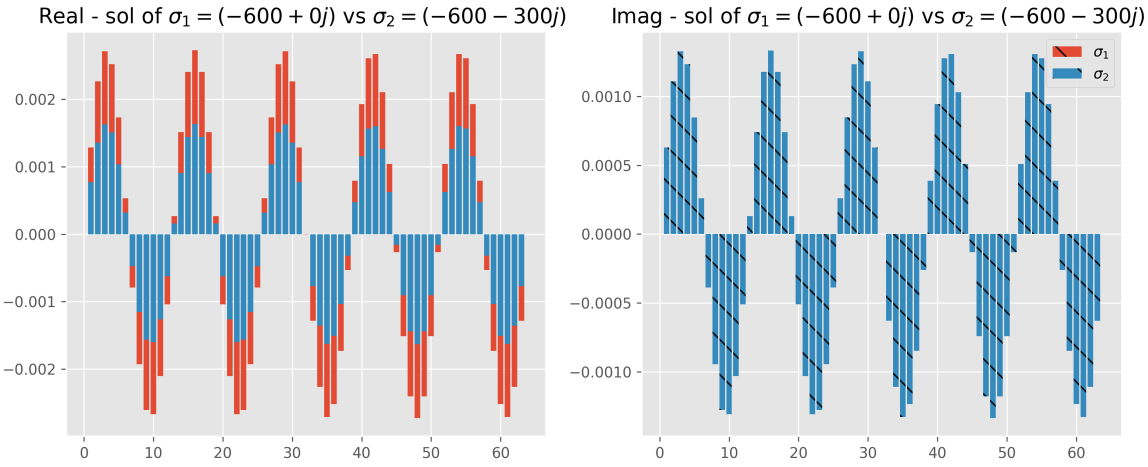

Figure 6: Exact solutions for $n = 64, f_n = w_{10}^n$ *comparing* $\sigma_1 = -600$ *and* $\sigma_2 = -600 - 300j$.

2.2 LFA analysis of the ω-Jacobi smoother

(a)
Already answered in previous question. ρ is still $|G(0)|$ almost the same reasoning.

$$|G(\theta)| = |a + b\cos(\theta) + c\cos(\theta)i| \tag{29}$$

with $a, b \in \mathbb{R}^+$ and $c \in \mathbb{R}$ still gets optimized when $\cos(\theta)$ gets optimized.
(b)
Not much is changed compared the real case.

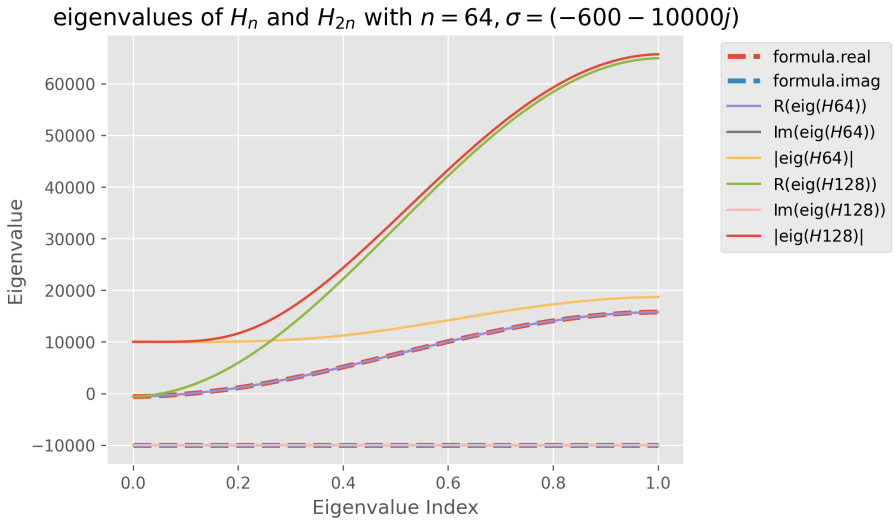

Figure 7: We sorted the eigenvalues and scaled the x-axis to make it easier to compare eigenvalues. Note that H_{2n} has twice the amount of eigenvalues then H_n.

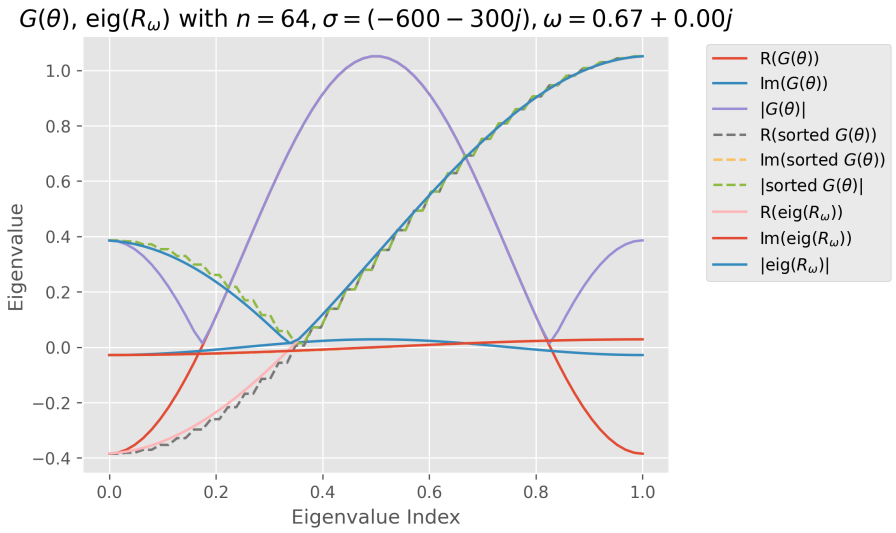

Figure 8: We sorted the eigenvalues and scaled the x-axis to make it easier to compare eigenvalues.

(c)
It is either $|G(\pi)|$ or $|G(\frac{\pi}{2})|$ see main.ipynb. For $\omega = 2/3$ they are roughly equal with $\mu = \frac{1}{3}$.
(d)
Eyeballing Figure 9, $\omega \approx 0.65$ is good.

2.3 Spectral analysis of the two-grid correction scheme

(a)
See Figure 10. We used the formula not numerical eigenvalues ...

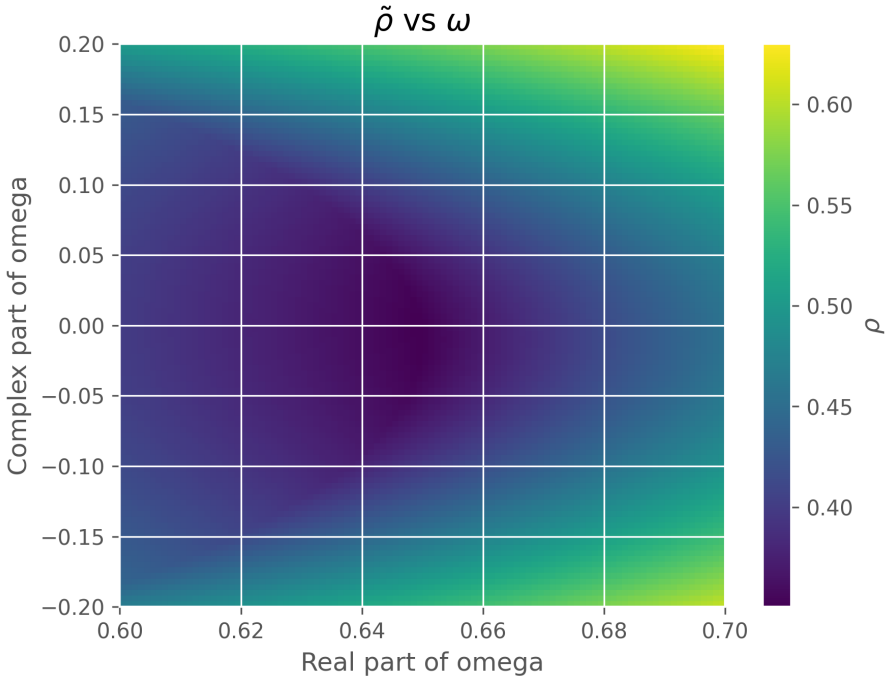

Figure 9

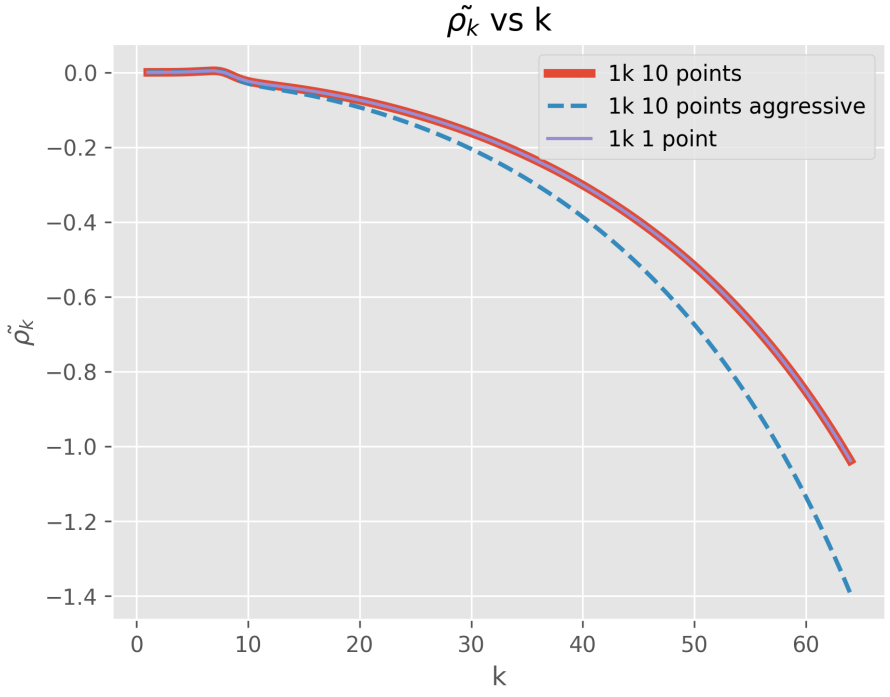

Figure 10

(b)
The instability in ρ_k dampens. Compare

$$\frac{\varepsilon + \beta j}{\tilde{\varepsilon} + \beta j} \text{ vs } \frac{-\varepsilon + \beta j}{\tilde{\varepsilon} + \beta j}.$$

with ε small, if $\beta = 0$, these are constants with different signs, for big enough β they are both roughly 1.

2.4 2D model problem

(a)

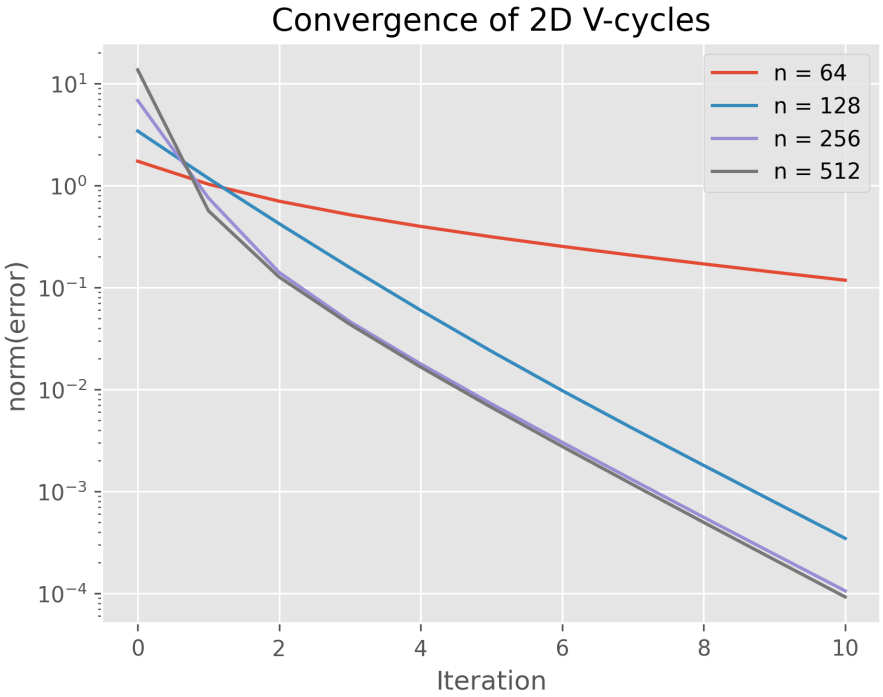

Figure 11: Convergence behavior of the V-cycles for solving the discretized Helmholtz equation in 2D with $\sigma = -600 - 300j$ and different n.

(b)
Less iterations are needed for the same amount of error. This is because σ the source of the problem get relatively smaller to n^2 in our convergence factors, asymptotically behavior should go back the Laplace problem.

2.5 Aggressive coarsening

(a)
Not sure here is our guess: (TG = two grid,FG = four grid)

$$FG = I - P_{2n}P_nH_n^{-1}R_{2n}R_{4n}H_{4n}. \tag{30}$$

Not sure what is meant by the eigenmode analysis but what we previously did does generalizes. The eigenmodes that are complementary with w_k^{4n} on the n grid are: $w_{4n-k}^{4n}, w_{2n-k}^{4n}, w_{2n+k}^{4n}$.
(b)
Our solver diverged. Basically we are skipping a smoothing step which makes the

interpolation worse. Also relevant is that convergence for this problem is better on larger grids. In the FG eigenmode analysis, interpolation error is worse and eigenvalues are less similar which suggest that only the smoothest modes of the errors get dampend. Accuracy drops but the trade off is that aggressive coarsening is less expensive about $\frac{1}{2^d}$ cheaper on everything but the operations on the base grid. (Half the geometric series is gone.)

3 Multigrid as a preconditioner for Krylov subspace methods

3.1 MG-GMRES for the indefinite Helmholtz problem

(a)

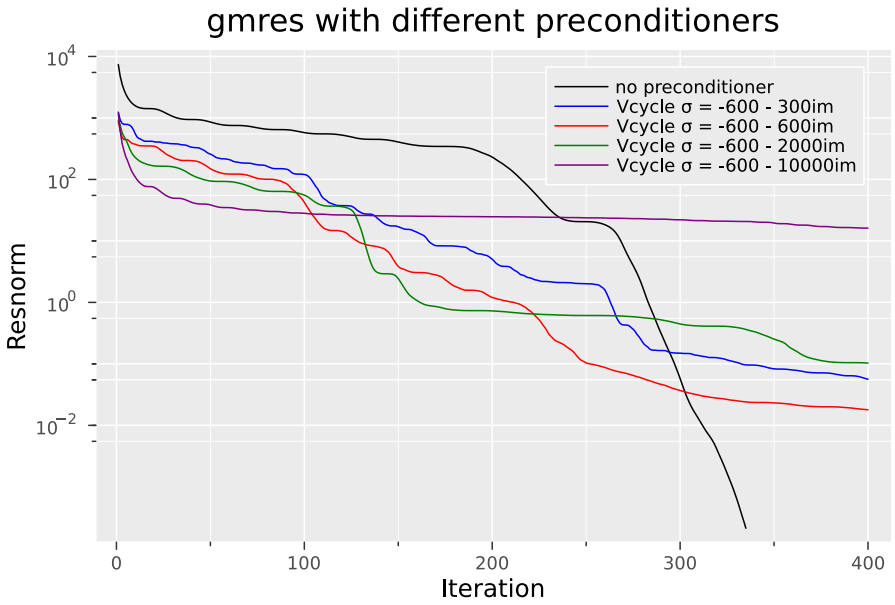

Figure 12: Convergence behavior of the norm of the residuals of gmres preconditioned with Vcyles with different σ for the Helmholtz equation with pointsource.

(b)
See (a).
(c)
Too large β results in a preconditioner too far from the inverse, too small β makes the vcycle behave poorly. $\beta = 0.5$ appears to be a good balance.

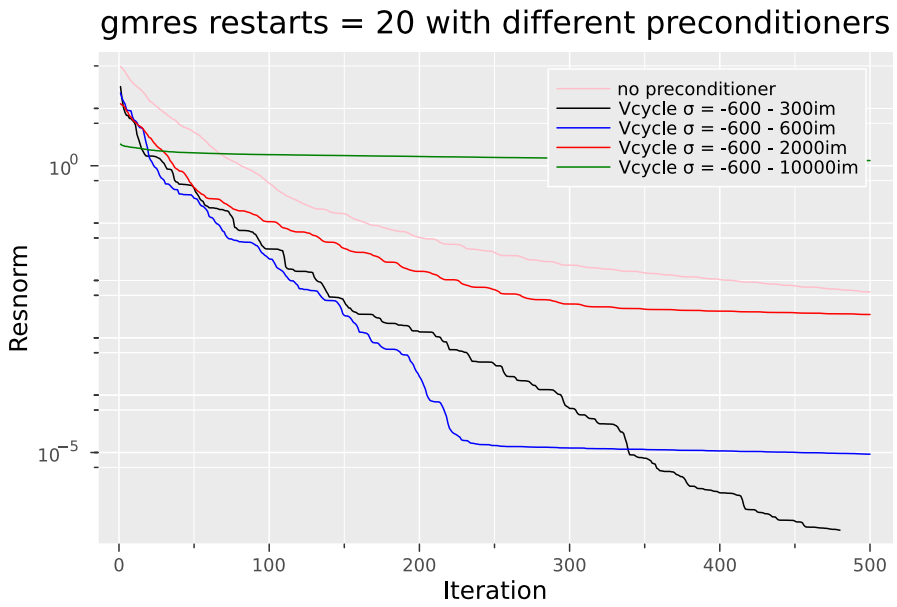

Figure 13: Convergence behavior of the norm of the residuals of restarted gmres preconditioned with Vcyles with different σ for the Helmholtz equation with a mixed wave basis source.